

RSC Advances



This is an *Accepted Manuscript*, which has been through the Royal Society of Chemistry peer review process and has been accepted for publication.

Accepted Manuscripts are published online shortly after acceptance, before technical editing, formatting and proof reading. Using this free service, authors can make their results available to the community, in citable form, before we publish the edited article. This *Accepted Manuscript* will be replaced by the edited, formatted and paginated article as soon as this is available.

You can find more information about *Accepted Manuscripts* in the [Information for Authors](#).

Please note that technical editing may introduce minor changes to the text and/or graphics, which may alter content. The journal's standard [Terms & Conditions](#) and the [Ethical guidelines](#) still apply. In no event shall the Royal Society of Chemistry be held responsible for any errors or omissions in this *Accepted Manuscript* or any consequences arising from the use of any information it contains.

ARTICLE

In situ growth of novel laminar-shaped Co_3S_4 as efficient counter electrode for dye-sensitized solar cells

Cite this:

DOI: 10.1039/x0xx00000x

Zhelu Hu, Kai Xia, Jing Zhang, Ziyang Hu, Yuejin Zhu*

Received 00th January 2012,
Accepted 00th January 2012

DOI: 10.1039/x0xx00000x

www.rsc.org/

Abstracts: Laminar cobalt sulfide (Co_3S_4) nanosheets are successfully deposited on fluorine doped tin oxide (FTO) substrates by a facile one-step hydrothermal method. When it was applied into dye sensitized solar cells as the counter electrode (CE), the laminar Co_3S_4 electrode, consisting of the interconnected nanosheets, exhibits prominent catalytic activity and outstanding metallic conductivity. It is the special structure that facilitates the electron transfer and reduces interface resistance. Under one sun (100 mW/cm^2) illumination, the dye-sensitized solar cell with the Co_3S_4 CE shows comparable photovoltaic conversion efficiency ($E_{\text{ff}} = 7.19\%$) to that with Pt CE ($E_{\text{ff}} = 7.27\%$). The results indicate that the in situ hydrothermal method and the prepared novel laminar Co_3S_4 CE is potential for developing low-cost and high-efficient counter electrode.

Introduction

In the past two decades, dye-sensitized solar cells (DSSCs) have attracted significant attention in transferring solar energy into electricity, due to their advantages of low-cost, easy-processing and high power conversion efficiency.¹⁻³ Generally, a typical DSSC has a sandwich structure, which consists of dye-sensitized mesoporous semiconductor nanocrystalline TiO_2 photoanode, an electrolyte containing aniodide (I^-)/triiodide (I_3^-) redox couple and a counter electrode. Of all the components, the counter electrode, as an indispensable part of DSSC, instantly extracts electrons from the external circuit and catalyzes the regeneration of I^- from I_3^- . Commonly the preferred CE is comprised of a thin layer of platinum (Pt) deposited on an FTO substrate, exhibited high catalytic activity for triiodide reduction, and excellent electrical conductivity.⁴ However, the extremely expensive price and low abundance of Pt undoubtedly limits its application for large-scale production of DSSCs.^{5, 6} It is very necessary to solve this issue by searching for other stable, cost-effective and environmentally friendly alternative materials to replace the noble Pt.

Recently, a large amount of potential free-Pt candidates have been introduced into DSSCs as the catalytic materials to substitute platinum, such as carbonaceous materials,⁷⁻⁹ conductive polymers¹⁰⁻¹² and inorganic compounds (transition-metal oxides,^{13, 14} nitrides,¹⁵ phosphides,¹⁶ carbides,¹⁷ sulfides^{18, 19} and selenides²⁰). In 2009, Grätzel et al. proposed that CoS nanoparticles, deposited electrochemically on flexible ITO/PEN films, matched the performance of Pt as a triiodide reduction catalyst in DSSCs.²¹ As is known, cobalt sulfides (CoS , Co_4S_3 ,

CoS_2 and Co_9S_8) are often applied in lithium ion batteries, electrochemical capacitors and other fields, due to their prominent characteristics of simple fabrication, abundant feedstock and excellent electrocatalytic activity.²² According to the slab band quantum computational principle, the calculated catalytic activity of Co_xS_y is analogous to Pt due to the corresponding surface structure which creates electron transfer pathways for oxygen reduction kinetics.²³ From that time, many researchers intensively focus on cobalt sulfides and the other variety of inorganic compounds. Moreover they pay closer attention to explore simple execution, low-cost and efficient preparation methods. A microspheric $\text{Co}_{8.4}\text{S}_8$ electrode was prepared by a simple solution processed method,²⁴ Optically transparent CoS counter electrode was synthesized through electro-deposition approach,²⁵ 3D CoS acicular nanorod arrays electrodes were prepared by chemical bath deposition method,²⁶ The Co_9S_8 Nanocrystal Ink was employed as cathode material to fabricate large-area DSSCs combined with spraying techniques.²⁷ All these approaches are very simple and have their own advantages for the preparation of counter electrodes, presenting remarkable photovoltaic performance.

With the purpose of improving the behavior of counter electrode, it is found that increasing the surface area of cathodic materials may provide more active sites, which is of great benefit for triiodide reduction reaction. For example, large specific surface area of FeS_2 nanorod electrode,²⁸ graphene-like $\text{Co}_{0.85}\text{Se}$ and $\text{Ni}_{0.85}\text{Se}$ electrodes,²⁹ hierarchical cobalt sulfide spindle electrodes³⁰ possess superior catalytic activity and exhibit excellent power conversion efficiency.

In this work, novel laminar cobalt sulfide nanosheets on FTO are fabricated by a simple one-step hydrothermal approach. The

obtained Co_3S_4 CE shows remarkable catalytic activity for reduction of I_3^- . The efficient performance is due to the special "laminar-like" nanosheets structure which possesses large surface area to make for electronic migration. To the best of our knowledge, it is the first time that the laminar-shaped Co_3S_4 is grown on a transparent conductive oxide (TCO) substrate as CE with one-step hydrothermal method. DSSC involved this special structure of Co_3S_4 electrode achieves 7.19% energy conversion efficiency, under AM1.5G simulated solar light ($100\text{mW}/\text{cm}^2$), which is comparable to that of DSSC based on conventional Pt CE (7.27%).

Experimental section

Preparation of counter electrodes

All chemical reagents were used as received without further purification. The typical procedure for Co_3S_4 counter electrode is as follows: Firstly, the transparent FTO glass substrates (NSG, Japan) were ultrasonically cleaned sequentially in deionized water, acetone, and ethanol for 10 min, respectively, and then stored in ethanol. Secondly, the preparation of Co_3S_4 nanosheets, directly grown on FTO substrates, adopted one-step hydrothermal method. $\text{CoCl}_2 \cdot 6\text{H}_2\text{O}$ (1.5 mmol, Aladdin) and thiourea powder (15 mmol, Aladdin) were dissolved in 80 mL of deionized water and stirred for 10 min until a clear and homogeneous pink solution was achieved. The whole solution was then transferred into a 100 mL Teflon-lined autoclave. A piece of cleaned FTO substrate was placed at an angle against the wall of the Teflon-liner autoclave with the conductive side facing down. The autoclave was sealed and heated in an oven at 140, 160 or 180 °C for 20 h and the reaction system was also maintained at 160 °C for 16 or 24 h, in that period without intentional control of ramping or cooling rate. The samples of which were denoted as T140-20h, T160-20h, T180-20h, T160-16h, T160-24h respectively.

When the process was completed, the prepared counter electrodes were removed from the solution, thoroughly washing several times with deionized water. After that, the shallow black Co_3S_4 electrodes were dried in a vacuum oven at 60 °C for 5 h.

Fabrication of the DSSCs

The TiO_2 anode was prepared as described previously.³¹ Prepared TiO_2 porous films were deposited onto FTO by doctor-blade technique. The electrode was gradually heated under an airflow at 200 °C for 5 min, at 325 °C for 5 min, at 375 °C for 5 min, and at 450 °C for 15 min, and finally, at 500 °C for 15 min. The thickness of the TiO_2 films were about 12 μm . The prepared TiO_2 electrode was immersed into a 0.5 mM N719 dye solution (acetonitrile and tert-butyl alcohol with volume ratio of 1:1). Then the electrolyte was a solution of 0.60 M BMII, 0.03 M I_2 , 0.10 M guanidinium thiocyanate and 0.50 M 4-tertbutylpyridine of acetonitrile and valeronitrile (volume ratio, 85:15). The dye-covered TiO_2 electrode, electrolyte and

Pt/ Co_3S_4 counter electrode were assembled to be a sandwich type cell to take the measurement.

Characterization and measurements

The morphologies of the Co_3S_4 were characterized by scanning electron microscopy (SEM; SU-70, Japan). The Co_3S_4 nanosheets were determined using X-ray diffraction analysis (XRD, D8 Advance, Bruker AXS, German) measured with $\text{Cu K}\alpha$ ($\lambda=0.154\text{ nm}$) at 50 kV and 40 mA over the two theta range 20° to 80°. Cyclic voltammetry (CV) was performed with an electrochemical workstation (Zennium, Germany) in a three-electrode setup, which consisted of the Pt/FTO or Co_3S_4 /FTO working electrode, a platinum wire counter electrode, and an Ag/AgCl reference electrode, immersing in acetonitrile electrolyte containing 10 mM LiI, 1 mM I_2 and 0.1 M LiClO_4 at a scan rate of 50 mV/s. Electrical impedance spectra (EIS) and Tafel polarization curves of the CEs were measured using the same electrochemical workstation (Zennium, Germany). The symmetrical dummy cells were assembled with two identical CEs filled with the same electrolyte as used in the DSSCs.^{32, 33} In EIS tests, the samples were scanned at zero bias potential and 10 mV amplitude over the frequency range 0.01–10⁵ Hz. The polarization measurements were performed at a scan rate of 50 mV/s. The photocurrent density-voltage (J-V) curve measurements were conducted with an AM 1.5 solar simulator equipped with a 1000 W xenon light source and AM 1.5G type filter (Newport, USA). The light intensity of the solar simulator was adjusted by using a Standard Si Cell. J-V curves were obtained by applying an external bias to the cell and measurements were recorded by a Keithley model 2400 digital source meter. A mask with a window of 0.16 cm² was also clipped onto the TiO_2 side to define the active area of the cell.

Results and discussion

Morphology and composition of CEs

After the hydrothermal procedure, the transparent FTO glass turns shallow black with semi-metallic luster. The XRD patterns of the prepared cobalt sulfides are shown in Fig. 1. The products demonstrate that all prepared cobalt sulfides own identical diffraction peaks, which can be well indexed to Co_3S_4 at 26.67°, 31.36°, 38.04°, 55.00° and 62.21° (JCPDS No. 42-1448). Due to growth of Co_3S_4 on FTO substrates, there are some peaks belong to the FTO substrate without any impurity phase. It should be noticed that the peak intensity grows higher for samples of T160-20h and T180-20h, indicating Co_3S_4 is better crystallized at reaction time of 20 h and temperature of 160 and 180 °C compared with other samples.

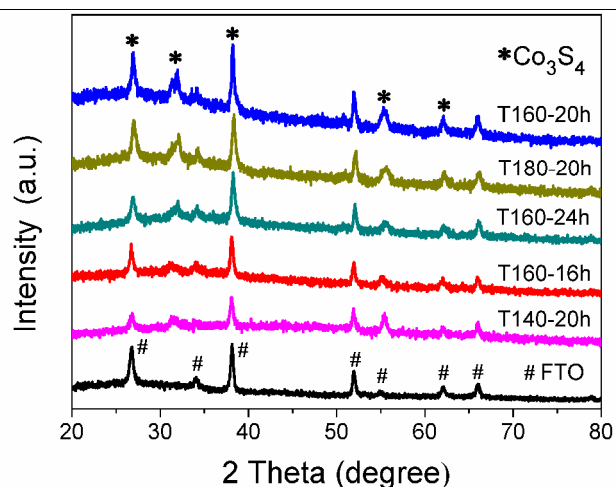


Fig.1 XRD patterns of T140-20h, T160-20h, T180-20h, T160-16h, T160-24h Co_3S_4 nanosheets on FTO substrates.

Fig.2 shows the SEM images of the Co_3S_4 nanostructures prepared by hydrothermal method under different reaction temperature or reaction time. As shown in Fig.2, with the increment of reaction time or reaction temperature, the small sized Co_3S_4 nanosheets gradually assembled into big and compact nanosheets. In Fig.2(a), the fabricated Co_3S_4 at low

temperature (140°C for 20h) presents a sparse nanosheets structure. With increasing temperature to 160°C for 20h, the nanosheets begin to grow bigger. By increasing the temperature to 180°C , the as-produced nanosheets transform into compact nano-block structure (Fig.2(e)), so that the electron transportation becomes more difficult. When the reaction condition happens at 160°C for 20h, the laminar-shaped Co_3S_4 , rarely seen in recent research, is directly deposited on FTO with unique special structure as shown in Fig.2(c), and the multilayer nanosheets can be obviously seen from the high magnification graph at top-view from Fig.2(c). We also find that T160-20h metal sulfides are connected or very close to each other to form conductive paths, which benefits for electron transfer from one particle to another.³⁴ Fig.2(f) reveals that the layer thickness of the fabricated T160-20h Co_3S_4 is 544nm thick. When the temperature controls at 160°C , the reduced reaction time of 16h results the agglomerate distributed Co_3S_4 products (Fig.2(b)). Then, with increased the reaction time to 24h (Fig.2(d)), the laminar-shaped Co_3S_4 nanosheets turn to more dense and compact. It is concluded the reaction condition of 160°C for 20h is most suitable for large surface area Co_3S_4 CE fabrication. The unique structure may offer high conductivity for fast electron transport and provide more interfacial active sites for electrolyte of triiodide reduction.

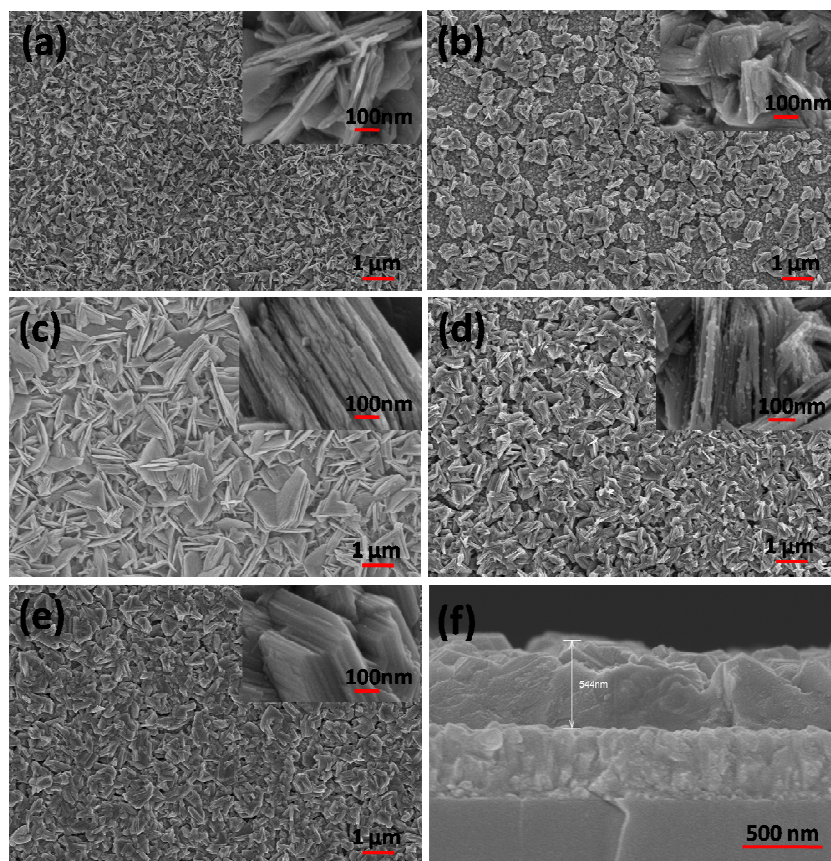


Fig.2 SEM images of microstructure of T140-20h (a), T160-16h (b), T160-20h (c), T160-24h (d), T180-20h (e) Co_3S_4 with high magnification inset, cross-sectional T160-20h Co_3S_4 (f).

ARTICLE

Electrocatalytic properties of CEs

Cyclic voltammetry (CV) is performed to investigate the electrocatalytic activity of CEs for the reduction of triiodide which is closely related with the photovoltaic performance.³⁵ Fig.3 shows the CV curves for Pt and Co₃S₄ electrodes prepared in different reaction time (T160°C-16, 20, 24h) and different reaction temperature (T20h-140, 160, 180°C), respectively. All the electrodes present two pairs of redox peaks, the left redox peaks corresponded to eq.(1) and the right ones corresponded to eq.(2), respectively:

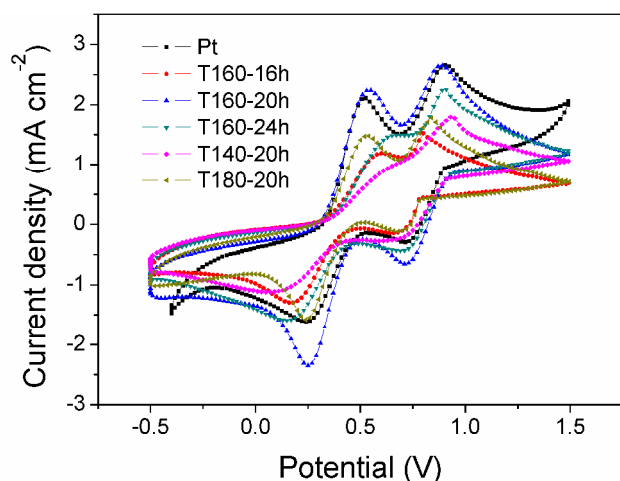


Fig.3 CV of I⁻/I₃⁻ redox system for different CEs at a scan rate of 50 mV/s cycling in electrolyte (10 mM LiI, 1 mM I₂, 0.1 M LiClO₄).

The peak currents and the peak-to-peak separation (E_{pp}) in cyclic voltammetry curves are two important parameters for comparing catalytic activities of different CEs.³⁶ Of which, E_{pp} is inversely correlated with the rate of the corresponding redox reaction. As shown in the Fig.3, T160-20h Co₃S₄ CE possesses similar profiles and positions of the two redox pairs in comparison with the Pt CE, hence comparable peak currents and E_{pp} value prove that the similar catalytic performance. The increased (T160-24h) or decreased (T160-16h) the reaction time results lower peak currents and wider E_{pp} , indicating the electrodes are inferior to Pt and T160-20h electrodes. Although the peak currents of T180-20h is slight lower, the E_{pp} is little narrower compared with Pt, which reveals that the

electrochemical catalysts of T180-20h Co₃S₄ electrode is close to Pt CE. Similarly, no apparent peak is observed for the T140-20h electrode in this potential interval (-0.5V to 1.5V), suggesting the reduction reaction of I₃⁻ to I⁻ is poor compared to Pt CE. According to the above results, we find the laminar T160-20h Co₃S₄ nanosheets possess narrower E_{pp} and higher peak currents and obviously show the best electrocatalytic activity for the reduction of I₃⁻. It is inferred that the catalytic property of each CE is closely related to the specific area nanosheets structure (Fig.2(c)), which also directly affects the DSSC performance and is well proved by conversion efficiencies (table 1).

Tafel polarization

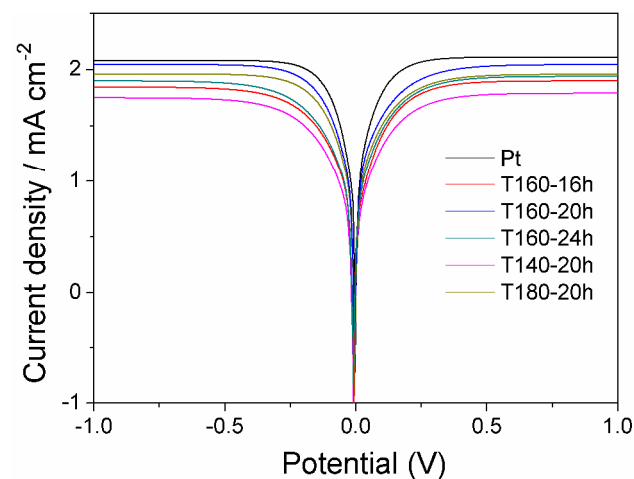


Fig.4 Tafel polarization curves of the symmetrical cells based on two identical CEs in the same electrolyte as that used in DSSCs at the scan rate of 50 mV/s.

The Tafel polarization is used to further reconfirm the catalytic activity of the samples. Fig.4 shows the Tafel polarization curves which were derived with the resemble dummy cells to verify the relative properties of laminar cobalt sulfide nanosheets.^{26, 37} From the Tafel zone, we can get the information about the exchange current density (J_0) and the limiting diffusion current density (J_{lim}), which are importantly related to electrochemical catalytic activities of CEs. The charge-transfer resistance (R_{ct}) is inversely proportional to J_0 (Eq.(3)), theoretically a larger slope in the anodic or cathodic branch suggests a higher exchange current density (J_0) on the electrode³⁸ with smaller R_{ct}

$$J_0 \rightarrow \frac{RT}{nFR_{ct}} \quad (3)$$

where R is gas constant, T is the temperature (298 K), F is Faraday constant, n is the number of electrons involved in the reduction of triiodide at the electrode, and R_{ct} is the charge transfer resistance. Among all the CEs, we know the T160-20h Co_3S_4 and Pt have the larger slopes than T140-20h, T160-16h, T160-24h and T180-20h Co_3S_4 , indicating that laminar Co_3S_4 and Pt have similar electrocatalytic activity, and smaller R_{ct} values for triiodide reduction on the electrode surfaces. Generally, the trends in J_0 for the different electrodes in the Tafel plot are in a good agreement with the CV measurements.

The limiting diffusion current density (J_{lim}) could also be estimated from the plots, when the gradient becomes zero. J_{lim} is determined by the diffusion velocity of the redox couple in the electrolyte and also reflects the electrocatalytic activity of the electrodes. Though T160-16h, T160-24h, T140-20h Co_3S_4 electrodes have parallel slopes, T140-20h Co_3S_4 electrodes has lower J_{lim} , suggesting that the T140-20h Co_3S_4 CE presents inferior electrocatalytic activity. According to the above result, the T160-20h Co_3S_4 shows the highest J_0 , J_{lim} and smallest R_{ct} value, and thus achieved highest catalytic activity. Consequently, we can conclude from the CV and Tafel polarization tests that laminar-shaped (T160-20h) Co_3S_4 CE possesses Pt-like electrocatalytic activity to catalyze the reduction of triiodide.

Photovoltaic performance of the cells

The photovoltaic performance of solar cells is characterized by measuring their current-voltage behaviour.^{39, 40} The J-V curves of the DSSCs with Pt, T140-20h, T160-20h, T180-20h, T160-16h, T160-24h as CEs, respectively are shown in the Fig.5, and the detailed photovoltaic parameters are summarized in Table 1. The DSSC based on Pt CE has an open-circuit voltage (V_{oc}) of 0.70 V, a short-circuit current density (J_{sc}) of 15.99 mA/cm^2 , a fill factor (FF) of 0.67, and a PCE of 7.27%. When the laminar-like structure cobalt sulfide T160-20h used as a CE, it obtains V_{oc} of 0.70V, J_{sc} of 15.34 mA/cm^2 , FF of 0.66, and a PCE of 7.19%, which reveals comparable properties with that of Pt CE. It is also quite clear that the performance is superior than that of DSSCs based on T140-20h (5.93%), T180-20h (6.94%) CEs, which is due to their lower J_{sc} . It indicates that the electro-catalytic activity is prominently originated from the synthesis of Co_3S_4 phase in optimum heated temperature. Furthermore, compared with the performance of T160-16h (6.43%) and T160-24h (6.55%), it is concluded that the optimal time of hydrothermal reaction is 20h. The photovoltaic performance is in accordance with the catalytic property which is determined by the nano structure and fabricated condition. The remarkable performance of T160-20h Co_3S_4 CE can be attributed to more available reaction sites from the large surface area of interconnected nanoplatelets as shown in SEM Fig.2(c).³⁰ It indicates that in situ growth of T160-20h cobalt sulfide on FTO is a potential candidate to replace Pt CE.

Table 1. Performance characteristics of DSSCs based on different CEs.

| CE | V_{oc} V | J_{sc} mA/cm^2 | FF | η % | R_s Ωcm^2 | R_{ct} Ωcm^2 |
|----------|---------------|-------------------------------------|------|-------------|------------------------------|---------------------------------|
| Pt | 0.70 | 15.99 | 0.67 | 7.27 | 1.15 | 1.88 |
| T160-16h | 0.69 | 14.06 | 0.65 | 6.43 | 1.79 | 6.98 |
| T160-20h | 0.70 | 15.34 | 0.66 | 7.19 | 2.13 | 2.16 |
| T160-24h | 0.70 | 14.41 | 0.64 | 6.55 | 3.41 | 6.03 |
| T140-20h | 0.68 | 13.04 | 0.67 | 5.93 | 2.46 | 10.66 |
| T180-20h | 0.70 | 14.83 | 0.66 | 6.94 | 2.29 | 2.37 |

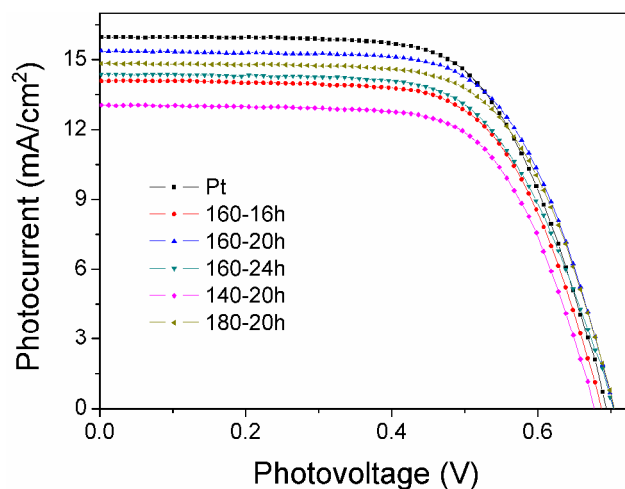


Fig.5 J-V curves of the cells based on different CEs.

EIS analysis

The inner electron transfer of the CE is further investigated by electrochemical impedance spectroscopy (EIS) measurements to evaluate the catalytic activity of the counter electrodes and explain the J_{sc} difference of the DSSCs.⁴¹⁻⁴³ The impedance analysis is performed on the symmetric cells constructed by two identical electrodes. The obtained Nyquist spectra and the equivalent circuit model are given in Fig.6.

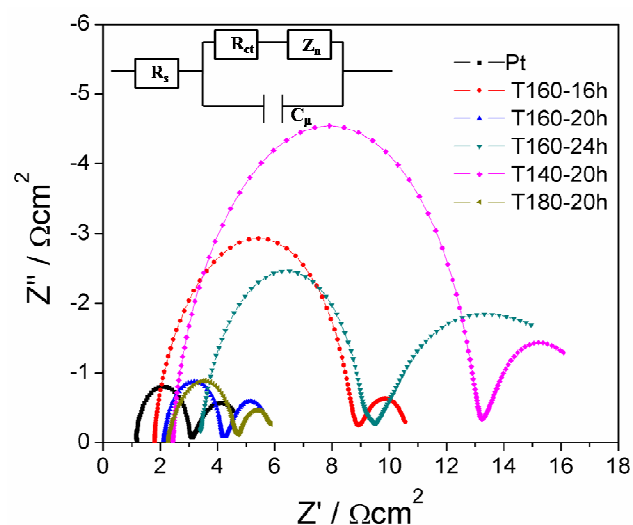


Fig.6 Nyquist plots of EIS for the symmetrical cells based on Pt, T140-20h, T160-16h, T160-20h, T160-24h and T180-20h Co_3S_4 CEs. The equivalent circuit model used to simulate the resultant spectra is shown in the inset.

In general, two hemispheres can be observed from the Nyquist plot, the left arc in the high frequency region reflects the charge-transfer resistance (R_{ct}) at the CE/electrolyte interface and the double layer capacitance (C_{μ}), meanwhile the right one in the low-frequency range represents the diffusion resistance (Z_n) of the redox couple in the electrolyte.⁴⁴ Moreover, the onset of intercept on the real axis indicates the total ohmic series resistance (R_s). By analysis the EIS spectra using the Z-view software, the charge-transfer resistance R_{ct} values of T140-20h, T180-20h, T160-16h, T160-24h are 10.66, 2.37, 6.98, 6.03 Ωcm^2 respectively, and the corresponding resistances are listed in Table 1. The R_{ct} is mainly related to the electrocatalytic activity for triiodine reduction, and a lower R_{ct} value indicates higher electrocatalytic activity. The R_{ct} value of the T160-20h Co_3S_4 electrode is 2.16 Ωcm^2 , which is close to that of the reference Pt electrode (1.88 Ωcm^2) and much lower than the other Co_3S_4 electrodes, indicating laminar cobalt T160-20h sulfide electrode owns excellent catalytic activity and electrical conductivity. The combination of lower R_{ct} , R_s and Z_n leads to a decrease in the total internal resistance than the other Co_3S_4 samples, comparable that to Pt CE, and thus leading to high J_{sc} and PCE. In view of Fig.2(c), the T160-20h possesses larger specific surface area, so suggesting the Co_3S_4 morphology and structure have a significant impact on the electron transfer through interface.⁴⁵ These EIS results are well accordance with the CV, Tafel polarization analysis and the photovoltaic performance of DSSCs.

Conclusions

In summary, laminar-shaped Co_3S_4 nanosheets are successfully grown on FTO substrate as Pt-free CE of DSSCs, via a facile one-pot hydrothermal method. The as-prepared Co_3S_4 lamellar structure not only shows high surface area for pervasion of electrolyte, but also exhibits excellent conductivity and catalytic activity. The prominent performance of dye sensitized solar cells based on cobalt sulfide counter electrode is prepared under the reaction condition of 160°C for 20h. Achieved the maximum PCE of Co_3S_4 CE is 7.19%, which is very close to that of Pt CE (7.27%). The laminar cobalt sulfide counter electrode is low cost, easy fabrication, meanwhile shows superior photovoltaic performance, demonstrating that it is a prospective and cost-effective candidate to realize large-scale industrialized production for DSSCs.

Acknowledgements

This work is supported by National Nature Science Foundation of China (contact grant number: 11174163, 11374168 and 51302137) and K. C. Wong Magna Fund, Ningbo University

Notes and references

Department of Physics, Ningbo University, Ningbo 315211, Zhejiang, China.
Fax: +86 574 87600744; Tel: +86 574 87600770; E-mail: zhuyuejin@nbu.edu.cn

1. B. O'regan and M. Grätzel, *nature*, 1991, 353, 737-740.
2. A. Yella, H. W. Lee, H. N. Tsao, C. Yi, A. K. Chandiran, M. K. Nazeeruddin, E. W. Diau, C. Y. Yeh, S. M. Zakeeruddin and M. Grätzel, *Science*, 2011, 334, 629-634.
3. M. Grätzel, *nature*, 2001, 414, 338-344.
4. N. Papageorgiou, W. Maier and M. Grätzel, *Journal of the electrochemical Society*, 1997, 144, 876-884.
5. B. O'Regan, D. T. Schwartz, S. M. Zakeeruddin and M. Grätzel, *Advanced Materials*, 2000, 12, 1263-1267.
6. C.-J. Yang, *Energy Policy*, 2009, 37, 1805-1808.
7. W. J. Lee, E. Ramasamy, D. Y. Lee and J. S. Song, *ACS applied materials & interfaces*, 2009, 1, 1145-1149.
8. Z. W. Kehan Yu, Haihui Pu, Ganhua Lu, Zheng Bo, Haejune Kim, Yuanyuan Qian, Erin Andrew, Shun Mao and Junhong Chen, *Journal of Materials Chemistry A*, 2013, 1, 188-193.
9. J. Z. Xueni Zhang, Yanzheng Cui, Jiangwei Feng, Yuejin Zhu, *J. APPL. POLYM. SCI.*, 2012, 128, 75-79.
10. Q. Tai, B. Chen, F. Guo, S. Xu, H. Hu, B. Sebo and X.-Z. Zhao, *ACS Nano*, 2011, 5, 3795-3799.
11. S. Ahmad, E. Dell'Orto, J.-H. Yum, F. Kessler, M. K. Nazeeruddin and M. Grätzel, *Chemical Communications*, 2012, 48, 9714-9716.
12. S. Peng, P. Zhu, Y. Wu, S. G. Mhaisalkar and S. Ramakrishna, *Rsc Advances*, 2012, 2, 652-657.
13. M. Wu, X. Lin, A. Hagfeldt and T. Ma, *Chem Commun (Camb)*, 2011, 47, 4535-4537.
14. Q. Zhang, Y. Liu, Y. Duan, N. Fu, Q. Liu, Y. Fang, Q. Sun and Y. Lin, *Rsc Advances*, 2014, 4, 15091-15097.
15. X. Zhang, X. Chen, S. Dong, Z. Liu, X. Zhou, J. Yao, S. Pang, H. Xu, Z. Zhang and L. Li, *Journal of Materials Chemistry*, 2012, 22, 6067-6071.
16. M. S. Wu and J. F. Wu, *Chem Commun (Camb)*, 2013, 49, 10971-10973.
17. M. Wu, X. Lin, A. Hagfeldt and T. Ma, *Angew Chem Int Ed Engl*, 2011, 50, 3520-3524.
18. W. Zhao, T. Lin, S. Sun, H. Bi, P. Chen, D. Wan and F. Huang, *Journal of Materials Chemistry A*, 2013, 1, 194-198.
19. M. Al-Mamun, H. Zhang, P. Liu, Y. Wang, J. Cao and H. Zhao, *Rsc Advances*, 2014, 4, 21277-21283.
20. Z. Zhang, S. Pang, H. Xu, Z. Yang, X. Zhang, Z. Liu, X. Wang, X. Zhou, S. Dong and X. Chen, *RSC Adv.*, 2013, 3, 16528-16533.
21. M. Wang, A. M. Anghel, B. t. Marsan, N.-L. Cevey Ha, N. Postrakulchote, S. M. Zakeeruddin and M. Grätzel, *Journal of the American Chemical Society*, 2009, 131, 15976-15977.
22. Q. Liu and J. Zhang, *CrystEngComm*, 2013, 15, 5087.
23. Y. Hou, D. Wang, X. H. Yang, W. Q. Fang, B. Zhang, H. F. Wang, G. Z. Lu, P. Hu, H. J. Zhao and H. G. Yang, *Nature communications*, 2013, 4, 1583.
24. H. K. Mulmudi, S. K. Batabyal, M. Rao, R. R. Prabhakar, N. Mathews, Y. M. Lam and S. G. Mhaisalkar, *Physical chemistry chemical physics : PCCP*, 2011, 13, 19307-19309.
25. S.-Y. Tai, C.-F. Chang, W.-C. Liu, J.-H. Liao and J.-Y. Lin, *Electrochimica Acta*, 2013, 107, 66-70.
26. C.-W. Kung, H.-W. Chen, C.-Y. Lin, K.-C. Huang, R. Vittal and K.-C. Ho, *ACS Nano*, 2012, 6, 7016-7025.

-
27. S.-H. Chang, M.-D. Lu, Y.-L. Tung and H.-Y. Tuan, *ACS Nano*, 2013, 7, 9443-9451.
 28. Q.-H. Huang, T. Ling, S.-Z. Qiao and X.-W. Du, *Journal of Materials Chemistry A*, 2013, 1, 11828.
 29. F. Gong, H. Wang, X. Xu, G. Zhou and Z. S. Wang, *Journal of the American Chemical Society*, 2012, 134, 10953-10958.
 30. G. Wang and S. Zhuo, *Physical chemistry chemical physics : PCCP*, 2013, 15, 13801-13804.
 31. S. Ito, T. N. Murakami, P. Comte, P. Liska, C. Grätzel, M. K. Nazeeruddin and M. Grätzel, *Thin Solid Films*, 2008, 516, 4613-4619.
 32. T. C. Wei, C. C. Wan and Y. Y. Wang, *Applied Physics Letters*, 2006, 88, 103122.
 33. C.-Y. Lin, J.-Y. Lin, J.-L. Lan, T.-C. Wei and C.-C. Wan, *Electrochemical and Solid-State Letters*, 2010, 13, D77.
 34. K. Imoto, K. Takahashi, T. Yamaguchi, T. Komura, J.-i. Nakamura and K. Murata, *Solar Energy Materials and Solar Cells*, 2003, 79, 459-469.
 35. Y. Wang, M. Wu, X. Lin, Z. Shi, A. Hagfeldt and T. Ma, *Journal of Materials Chemistry*, 2012, 22, 4009-4014.
 36. J. D. Roy-Mayhew, D. J. Bozym, C. Punckt and I. A. Aksay, *ACS Nano*, 2010, 4, 6203-6211.
 37. M. Wu, X. Lin, Y. Wang, L. Wang, W. Guo, D. Qi, X. Peng, A. Hagfeldt, M. Gratzel and T. Ma, *Journal of the American Chemical Society*, 2012, 134, 3419-3428.
 38. Z. Li, F. Gong, G. Zhou and Z.-S. Wang, *The Journal of Physical Chemistry C*, 2013, 117, 6561-6566.
 39. W. Zhao, X. Zhu, H. Bi, H. Cui, S. Sun and F. Huang, *Journal of Power Sources*, 2013, 242, 28-32.
 40. J.-Y. Lin, J.-H. Liao and S.-W. Chou, *Electrochimica Acta*, 2011, 56, 8818-8826.
 41. G. Yue, J. Wu, Y. Xiao, M. Huang, J. Lin and J.-Y. Lin, *Journal of Materials Chemistry A*, 2013, 1, 1495.
 42. J. Wu, G. Yue, Y. Xiao, M. Huang, J. Lin, L. Fan, Z. Lan and J. Y. Lin, *ACS applied materials & interfaces*, 2012, 4, 6530-6536.
 43. Y. C. Wang, D. Y. Wang, Y. T. Jiang, H. A. Chen, C. C. Chen, K. C. Ho, H. L. Chou and C. W. Chen, *Angew Chem Int Ed Engl*, 2013, 52, 6694-6698.
 44. S. Yun, M. Wu, Y. Wang, J. Shi, X. Lin, A. Hagfeldt and T. Ma, *ChemSusChem*, 2013, 6, 411-416.
 45. Y. Zhao, A. Thapa, Q. Feng, M. Xi, Q. Qiao and H. Fong, *Nanoscale*, 2013, 5, 11742-11747.